

1     **Application of the AI2 Climate Emulator to E3SMv2’s**  
2     **global atmosphere model, with a focus on precipitation**  
3     **fidelity**

4             **James P. C. Duncan<sup>1</sup>, Elynn Wu<sup>2</sup>, Jean-Christophe Golaz<sup>3</sup>, Peter M.**  
5             **Caldwell<sup>3</sup>, Oliver Watt-Meyer<sup>2</sup>, Spencer K. Clark<sup>2</sup>, Jeremy McGibbon<sup>2</sup>,**  
6             **Gideon Dresdner<sup>2</sup>, Karthik Kashinath<sup>4</sup>, Boris Bonev<sup>4</sup>, Michael S. Pritchard<sup>4</sup>,**  
7             **and Christopher S. Bretherton<sup>2</sup>**

8                             <sup>1</sup>University of California, Berkeley

9                             <sup>2</sup>Allen Institute for Artificial Intelligence (AI2), Seattle, USA

10                            <sup>3</sup>Lawrence Livermore National Laboratory, Livermore, California, USA

11                            <sup>4</sup>NVIDIA, Santa Clara, California, USA

12     **Key Points:**

- 13             • The ACE weather-climate emulator yields an accurate climate when trained on  
14             EAMv2, E3SMv2’s global atmosphere model.
- 15             • Time-mean biases vs. EAMv2 in diverse atmospheric fields are similar to those  
16             seen before for ACE applied to the FV3GFS atmospheric model.
- 17             • ACE captures the space-time organization of EAMv2 precipitation well, with a  
18             much smaller time-mean bias than EAMv2’s observational bias.

---

Corresponding author: James Duncan, [jpduncan@berkeley.edu](mailto:jpduncan@berkeley.edu)

## 19 Abstract

20 Can the current successes of global machine learning-based weather simulators be gen-  
 21 eralized beyond two-week forecasts to stable and accurate multiyear runs? The recently  
 22 developed AI2 Climate Emulator (ACE) suggests this is feasible, based upon 10-year sim-  
 23 ulations trained on a realistic global atmosphere model using a grid spacing of approx-  
 24 imately 110 km and forced by a repeating annual cycle of sea-surface temperature. Here  
 25 we show that ACE, without modification, can be trained to emulate another major at-  
 26 mospheric model, EAMv2, run at a comparable grid spacing for at least ten years with  
 27 similarly small climate biases. ACE accurately reproduces EAMv2’s frequency distribu-  
 28 tion of daily-mean precipitation, its time-mean spatial pattern of precipitation, and its  
 29 space-time structure of tropical precipitation, including the Madden-Julian Oscillation.  
 30 Moreover, ACE’s climate biases with respect to EAMv2 are substantially smaller than  
 31 EAMv2’s own biases compared to the observed historical average surface precipitation  
 32 rate and top-of-atmosphere radiative fluxes.

## 33 Plain Language Summary

34 Traditional methods to predict the weather use mathematical models of the Earth’s at-  
 35 mosphere that are costly to run. However, “data-driven” weather prediction methods,  
 36 which learn to predict future weather directly from data on past weather, have come to  
 37 match or even beat traditional methods and do so with much less running cost. In con-  
 38 trast to weather prediction where the goal is to predict the weather in the near future,  
 39 in *climate modeling* the goal is to study the Earth’s long-term weather trends under dif-  
 40 ferent possible future scenarios for many years into the future. Until the introduction  
 41 of the AI2 Climate Emulator (ACE), a recent data-driven method for climate modeling,  
 42 no data-driven method could match traditional climate models. In this work we test ACE’s  
 43 climate modeling skills and find that it is able to faithfully mimic a traditional model  
 44 of the climate when looking at patterns of rainfall around the globe and in the tropics.  
 45 With ACE, we can study the potential future of Earth’s climate under many more sce-  
 46 narios and with much lower cost than ever before.

## 47 1 Introduction

48 In recent years, the field of numerical weather prediction has undergone a significant trans-  
 49 formation, with researchers and institutions worldwide embracing machine learning (ML)  
 50 based techniques to make weather forecasts (Pathak et al., 2022; Lam et al., 2023; Bi  
 51 et al., 2023; Ben-Bouallegue et al., 2023). Notably, the European Centre for Medium-  
 52 Range Weather Forecasts (ECMWF) unveiled an Artificial Intelligence based Forecast-  
 53 ing System (AIFS) as a new companion to their physics-based numerical weather pre-  
 54 diction model (IFS). The shift from solely physics-based numerical weather prediction  
 55 to integrating ML-based systems has sparked considerable excitement within the scien-  
 56 tific community. While most studies have focused on short to medium-range weather fore-  
 57 casts (up to 14 days), the AI2 Climate Emulator (ACE) has demonstrated the ability  
 58 to emulate an existing global atmosphere model, FV3GFS, at climate timescales (Watt-  
 59 Meyer et al., 2023) by accurately simulating weather variability and deriving climate from  
 60 the statistics of the simulated weather, as do conventional global climate models. For  
 61 this reason we call ACE a weather-climate emulator, to distinguish it from much sim-  
 62 pler surrogate models that bypass weather simulation. Such models can instead be based  
 63 on global or large-scale budget equations, e.g. the Model for the Assessment of Greenhouse-  
 64 Gas Induced Climate Change (MAGICC) (Meinshausen et al., 2011) used in IPCC as-  
 65 sessment reports (e.g. Sec. 8.8.2 of IPCC (2013)), in which a few parameters are tuned  
 66 to give the same climate sensitivity, ocean heat uptake, and other salient global prop-  
 67 erties as a target global climate model. Alternatively, ML-based surrogate models such  
 68 as ClimaX (Nguyen et al., 2023) directly predict monthly climate evolution.

69 ACE approximately conserves mass and moisture, and accurately predicts the climatol-  
 70 ogy of key variables throughout the depth of the atmosphere. ACE can make a decade-  
 71 long simulation in one hour of wall clock time of one A100 GPU, making it 100 times  
 72 faster and more energy-efficient than FV3GFS run at a similar grid spacing.

73 Inspired by the achievements of ACE, in this paper we investigate its generalizability to  
 74 emulating a different global atmosphere model, the E3SM Atmosphere Model version 2  
 75 (EAMv2). EAMv2 is the atmospheric component of the U.S. Department of Energy’s  
 76 Energy Exascale Earth System Model version 2 (E3SMv2) (Golaz et al., 2022). As con-  
 77 figured for this study, EAMv2 fluid dynamics uses a grid spacing of approximately 110  
 78 km, like the FV3GFS implementation used for ACE. While FV3GFS is based on a finite-  
 79 volume dynamical core with 64 vertical layers, EAMv2 uses a spectral-element approach  
 80 with 72 layers while other processes use a finite-volume grid that divides each element  
 81 into  $2 \times 2$  cells of equal size, giving a horizontal resolution of 165 km (Hannah et al., 2021).  
 82 The physical parameterizations of EAMv2 are also substantially different than those of  
 83 FV3GFS.

84 We also analyze the emulation of precipitation in more detail than Watt-Meyer et al. (2023),  
 85 including its time-mean geographic distribution, its frequency distribution of daily vari-  
 86 ability, and its organization in the tropics. A final goal of this work is to bring aware-  
 87 ness of ACE and ML-based climate emulation into the traditional climate modeling lit-  
 88 erature.

## 89 2 Data and Methods

### 90 2.1 EAMv2 Dataset

91 Our training data is derived from 6-hourly outputs of a 73-year simulation of EAMv2,  
 92 a model described in detail in Section 2.1 of Golaz et al. (2022). The simulation is con-  
 93 figured to run with the “F2010” component set<sup>1</sup>, forcing the model with perpetual 2010  
 94 greenhouse gas concentrations and emissions of aerosols and precursors, along with an  
 95 annually repeating cycle of sea surface temperature and sea ice derived from the observed  
 96 2005-2014 average. The initial 11 years are discarded as spinup because the EAMv2 strato-  
 97 sphere is equilibrating; the following 42 years are used for training; the subsequent 10  
 98 years are used for validation; and the final 10 years are reserved for evaluating EAMv2’s  
 99 internal decadal variability. This simulation is performed on the E3SM Chrysalis clus-  
 100 ter, achieving 24 simulated years per day using 30 nodes. See Text S2 for a comparison  
 101 of the computational efficiencies of EAMv2 and ACE.

102 We make several other design choices following ACE (Watt-Meyer et al., 2023). First,  
 103 we perform a conservative regridding from the native EAMv2 output to a  $1^\circ$  Gaussian  
 104 grid to ensure compatibility with the underlying Spherical Fourier Neural Operator (SFNO)  
 105 architecture (Bonev et al., 2023). Second, we filter the data with a spherical harmonic  
 106 transform (SHT) round-trip to help eliminate artifacts in the high latitudes. Third, to  
 107 reduce the emulator’s memory footprint, we coarsen the vertical model-level coordinate  
 108 from the native 72 down to 8 layers. For more details see Table S2.

### 109 2.2 ACE Training Overview

As described by Watt-Meyer et al. (2023), ACE is a modified version of NVIDIA’s open-  
 source FourCastNet global atmospheric emulator (Pathak et al., 2022) that employs the  
 SFNO architecture for efficient spatial information exchange (Bonev et al., 2023). Much  
 as traditional physics-based numerical models of atmospheric dynamics recursively step  
 forward the atmospheric state  $X_t$  at time  $t$ , ACE is trained to autoregressively gener-

<sup>1</sup> <https://acme-climate.atlassian.net/wiki/spaces/DOC/pages/961250902/F2010C5-CMIP6-LR>

ate predictions of the atmospheric state at time  $t + \delta t$ :  $\hat{X}_{t+\delta t}$ . We use  $\delta t = 6$  hours and minimize the average “one-step” loss over a random batch  $\mathcal{B}$  of initial condition times  $t$ :

$$\frac{1}{|\mathcal{B}|} \sum_{t \in \mathcal{B}} \frac{\|\hat{X}_{t+\delta t} - X_{t+\delta t}\|_2}{\|X_{t+\delta t}\|_2}$$

110 Whereas FourCastNet uses identical input and output variables and trains a separate  
 111 model to predict diagnostic variables (Pathak et al., 2022), ACE uses a set of prognos-  
 112 tic variables which are both inputs and outputs, a set of specified forcing input variables  
 113 such as insolation and sea surface skin temperature which are exogenous to the dynam-  
 114 ical system, and a set of diagnostic variables which are incorporated in the training loss  
 115 but are output-only. This and a variety of other improvements enable ACE, unlike past  
 116 weather emulators, to produce stable, skillful, more interpretable multiyear emulations  
 117 of the target model. For more details see Table S3, Watt-Meyer et al. (2023), and Bonev  
 118 et al. (2023).

### 119 3 Results

120 Watt-Meyer et al. (2023) provide a holistic evaluation of ACE’s physical consistency when  
 121 trained on 100 years of FV3GFS simulation outputs in terms of physical budgets and  
 122 time- and global-mean biases and pattern errors.

123 Section 3.1 shows a similar analysis of ACE’s global- and time-mean absolute bias and  
 124 root mean square error (RMSE) metrics on EAMv2. This analysis shows that ACE pro-  
 125 duces a similarly high-quality emulation of the climatology of EAMv2 as for FV3GFS,  
 126 demonstrating that ACE’s training methodology generalizes across reference models of  
 127 comparable grid resolution with different dynamical cores and physical parameterizations.  
 128 In the remainder of Section 3, we present some key metrics of how well ACE emulates  
 129 EAMv2’s precipitation variability over the 10 year validation period, a topic not docu-  
 130 mented in detail by Watt-Meyer et al. (2023).

#### 131 3.1 Global- and time-mean biases and RMSE

132 In Figure 1, we compare ACE’s climatological skill to that of an unseen EAMv2 refer-  
 133 ence dataset, years 64–73 of the EAMv2 simulation run. Both ACE and the reference  
 134 are evaluated against the validation target years 54–63. The reference values give a ‘noise  
 135 floor’ estimate, computed as the difference of time means from a single pair of ten-year  
 136 segments of the reference simulation. Different pairs of ten-year periods would give dif-  
 137 ferent estimates for each output, with a scatter of positive-definite RMSEs and zero-centered  
 138 biases. For every output variable, we compute global-mean bias and spatial RMSE as  
 139 in Watt-Meyer et al. (2023) equations (6) and (7), respectively. Figure 1 also includes  
 140 the previously reported values for ACE trained and evaluated on FV3GFS simulation  
 141 outputs.

142 ACE’s time-mean RMSEs are comparable to the estimated noise floors for the reference  
 143 set, falling within a factor of two for many important lower-tropospheric fields and within  
 144 the same order of magnitude in all but a handful of cases. Global- and time-mean bi-  
 145 ases are also quite small in real terms and fall within one to two orders of magnitude of  
 146 the single-pair estimates of the EAMv2 reference dataset biases, with some noted excep-  
 147 tions such as surface pressure (top row in Figure 1). Global-mean surface pressure is the  
 148 sum of dry air mass (which should be conserved) and a much lesser water mass (which  
 149 is exchanged with the underlying ocean and land surface). In EAMv2, the 10-year mean  
 150 of this quantity is tightly constrained, varying little between different decadal samples  
 151 (i.e. small absolute bias in Figure 1). The current version of ACE does not enforce ex-  
 152 act global conservation equations for dry air and water and this causes larger temporal  
 153 drifts in global mean surface pressure when emulating both EAMv2 and FV3GFS. Nev-



**Figure 1.** Global- and time-mean absolute bias (left panel) and RMSE (right panel) metrics for all output variables, averaged over the 10 year validation period. From top to bottom, prognostic variables are listed first with diagnostic variables starting with *RSW*. Metrics computed on ACE EAMv2 outputs (“ACE-EAMv2”) are compared against: equivalent metrics for the “ACE-FV3GFS” model of (Watt-Meyer et al., 2023) with respect to the 10-year FV3GFS validation set; the best-case scenario EAMv2 metrics (“Reference”), as in Figure 3. Metrics are plotted with log scaling and units are given on the right margin for clarity.

154 ertheless, ACE produces a realistic time-mean map of surface pressure (not shown). With  
 155 a 10 year global-time-mean of  $-11$  Pa the magnitude of ACE’s surface pressure bias is  
 156 only around 0.01% of the typical surface pressure on Earth.

157 Overall, we find that with 42 years of training data, ACE is able to learn a representa-  
 158 tion of EAMv2 in terms of these metrics that is of similarly high quality to the results  
 159 obtained for FV3GFS using 100 years of training data. In what follows, we analyze the  
 160 frequency distribution of daily precipitation and time-mean spatial bias patterns of pre-  
 161 cipitation together with highly correlated top-of-atmosphere radiative fluxes. Then we  
 162 examine the spectrum and temporal evolution of tropical precipitation variability be-  
 163 tween  $15^\circ\text{S}$  and  $15^\circ\text{N}$ .

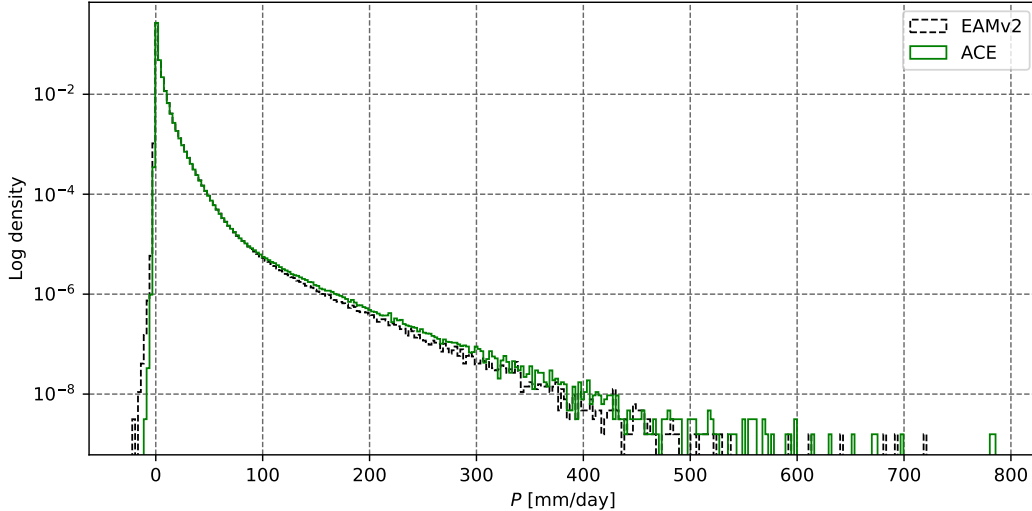


**Figure 2.** Frequency distribution of daily mean precipitation across all grid points over 10 years.

### 164 3.2 Precipitation density and spatial bias patterns

165 Establishing the precipitation extremes possible under various forcing scenarios is an im-  
 166 portant task for any climate model. Changes in the spatial distribution of time-mean  
 167 precipitation under a range of possible future climate scenarios also inform many aspects  
 168 of water-resource planning. Below, we examine ACE’s ability to match EAMv2 in terms  
 169 of (1) the frequency distribution of precipitation and (2) patterns of spatial bias in time-  
 170 mean precipitation and strongly associated top-of-atmosphere fluxes.

171 Figure 2 shows the frequency distribution of daily precipitation in EAMv2 (black, dashed  
 172 line) and ACE, including all grid points, over the 10 year validation period. Note that  
 173 both the target and generated precipitation fields have a small number of negative val-  
 174 ues due to the spherical harmonic transform round-trip applied to the data, an impor-  
 175 tant data preprocessing step that removes polar artifacts as explained in Watt-Meyer  
 176 et al. (2023). Overall, we see that ACE captures EAMv2’s precipitation distribution well,  
 177 including at the extreme upper quantiles. ACE’s ability to capture precipitation extremes  
 178 is an encouraging sign of the usefulness of deep learning GCM emulation for downstream  
 179 climate science tasks.

180 Figure 3 shows 10 year time-mean spatial bias patterns of precipitation and two highly  
 181 correlated fields: top-of-atmosphere upward short- and longwave radiative fluxes. The  
 182 left column labeled “EAMv2 vs. observation” displays the bias patterns observed when  
 183 comparing the EAMv2 simulation temporal mean over the validation years 54–63 to his-  
 184 torical observations. The observed precipitation comes from the Global Precipitation Cli-  
 185 matology Project (GPCP) (Huffman et al., 2023) version 3.2 and corresponds to the pe-  
 186 riod 1983–2021. The observed fluxes are from Clouds and the Earth’s Radiant Energy  
 187 System (CERES) Energy Balanced and Filled (EBAF) (Loeb et al., 2018) version 4.1,  
 188 over the period 2001–2018. In the right column, the corresponding validation target em-  
 189 ulation outputs from ACE, initialized from the first timepoint of year 54, are compared  
 190 against EAMv2. This way we can get a sense of the magnitude of ACE’s emulation bi-  
 191 ases relative to EAMv2’s observational biases.

192 The time-mean precipitation biases of ACE vs. EAMv2 range from  $-2.5$  to  $3.7$  mm/day  
 193 depending on location. The global spatial RMSE of time-mean precipitation is a remark-

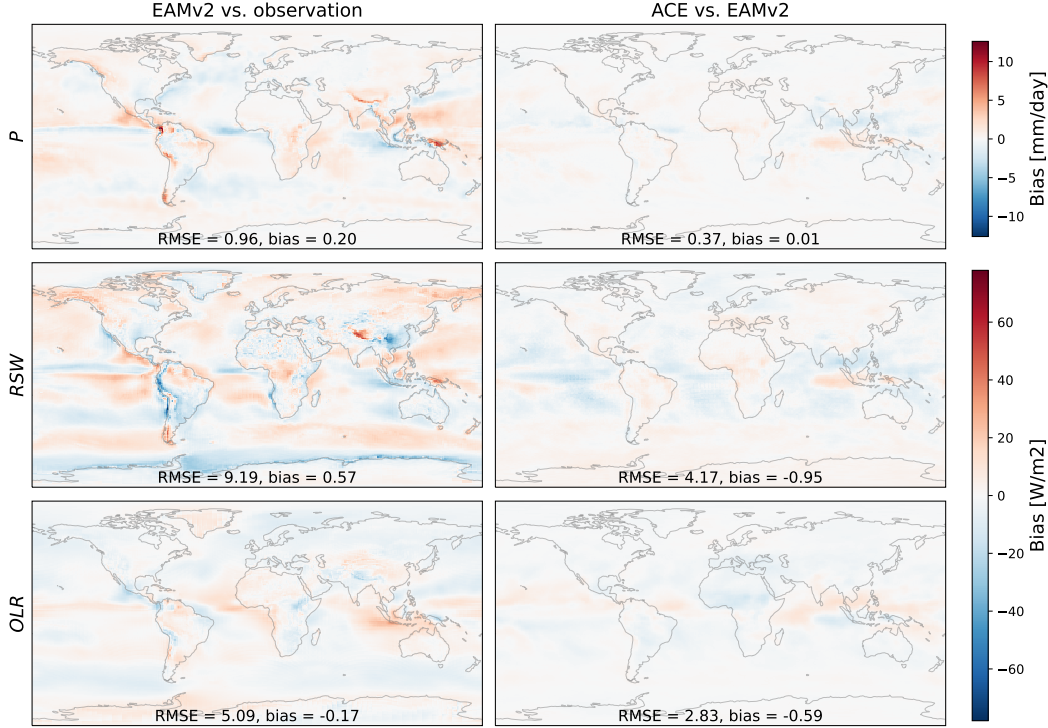


**Figure 3.** Temporal average of biases for surface precipitation rate (top row), outgoing top-of-atmosphere shortwave (RSW, middle row) and longwave (OLR, bottom row) radiative fluxes. The right column shows the mean spatial distribution of ACE biases vs. EAMv2, comparing the generated 6-hourly outputs to the corresponding simulation targets for the same timestep. The left column compares EAMv2 to the observed temporal mean (from GPCP for precipitation and CERES-EBAF for radiation; see main text.)

ably small 0.37 mm/day, which is comparable to the value of 0.46 reported in Watt-Meyer et al. (2023). EAMv2 observational biases lie between  $-6.5$  and  $12.6$  mm/day (Figure 3) with a RMSE of 0.96 mm/day. Thus ACE emulates EAMv2 precipitation patterns much better than EAMv2 can simulate them.

OLR biases follow an expected inverse relationship with precipitation biases, a good sign of ACE’s ability to emulate the radiative effects of precipitating cloud systems with cold cloud tops. Their spatial pattern RMSE is only  $2.8$  W/m<sup>2</sup>, with a global-mean bias of  $-0.59$  W/m<sup>2</sup>. ACE’s shortwave biases are larger, with a spatial pattern RMSE of  $4.2$  W/m<sup>2</sup> and a global-mean bias of  $-0.95$  W/m<sup>2</sup>. They are not just associated with deep precipitating cloud systems, but also ‘dim’ subtropical trade cumulus regimes, ‘bright’ Southern Ocean clouds, and excessive reflected shortwave radiation over Antarctica. As with precipitation, these emulation biases are small in comparison to EAMv2’s observational biases. See Table S1 for additional summary metrics.

### 3.3 Tracking tropical precipitation and the MJO

Most tropical precipitation falls from organized deep convective systems, including tropical cyclones, the Madden Julian Oscillation (MJO), and diverse convectively-coupled waves. Thus it is important that global atmospheric models accurately represent the space-

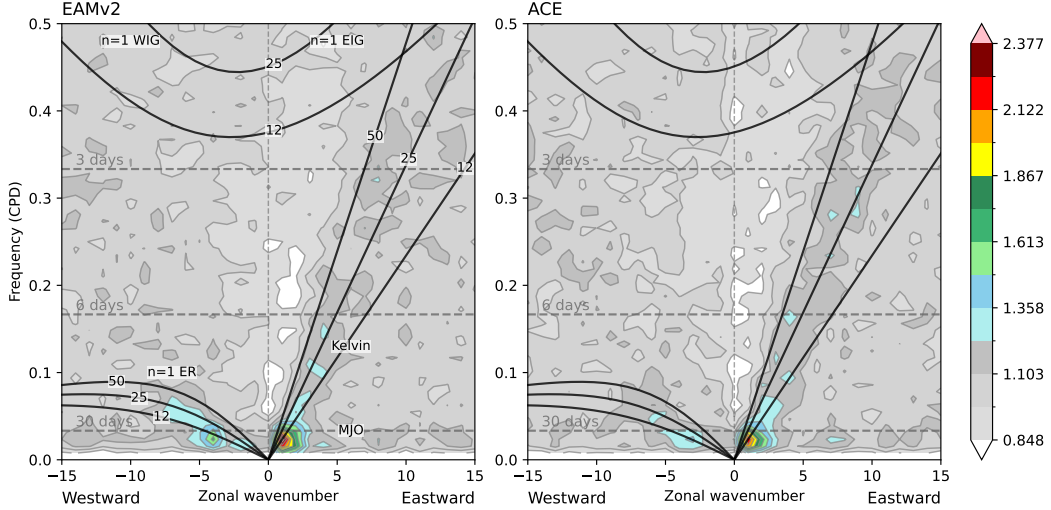


**Figure 4.** Normalized symmetric component of the wavenumber-frequency spectrum of daily-mean precipitation over a 10 year period for (left) withheld EAMv2 simulation output and (right) corresponding outputs from ACE. As with Figure 17 of Golaz et al. (2022), we label prominent wave types in the left panel and plot shallow water dispersion curves for equivalent depths 12, 25, and 50 m as solid black lines. ER = equatorial Rossby; EIG = eastward inertia-gravity; WIG = westward inertia-gravity.

211 time organization of tropical precipitation, and that an emulator of such a model repli-  
 212 cates the organization of its tropical precipitation.

213 The wavenumber-frequency spectrum (Wheeler & Kiladis, 1999) of daily-mean precipi-  
 214 tation meridionally averaged over  $15^{\circ}\text{S}$ - $15^{\circ}\text{N}$  is a widely used diagnostic of the large-  
 215 scale organization of tropical precipitation. In Figure 4, we plot the normalized symmet-  
 216 ric component of this wavenumber-frequency spectrum over the 10 year validation pe-  
 217 riod for the target EAMv2 simulation data and the corresponding outputs from ACE.  
 218 EAMv2’s spectrum is the appropriate ground truth against which to evaluate ACE, and  
 219 the emulator broadly captures EAMv2’s precipitation variability.

220 Some minor discrepancies include slightly reduced power in the MJO and the equato-  
 221 rial Rossby wave, the latter also peaking at a lower wavenumber in ACE compared to  
 222 EAMv2. Figure S2 provides a closer look at these features. As noted by Golaz et al. (2022),  
 223 compared to satellite retrievals of the historical period, EAMv2’s spectrum has weaker  
 224 normalized spectral power in the wavenumber-frequency bands corresponding to the MJO  
 225 and the equatorial Rossby wave and severely underestimates precipitation variability as-  
 226 sociated with Kelvin and westward inertia-gravity waves. By construction, a perfect emu-  
 227 lator should inherit these biases.

228 The Madden-Julian Oscillation (MJO) is a convectively-coupled Earth-spanning atmo-  
 229 spheric oscillation that is characterized by a large eastward-propagating band of anom-  
 230 alous precipitation in the tropics (Madden & Julian, 1971; Zhang, 2005). It is the most  
 231 regular and predictable sub-seasonal oscillation of the Earth’s atmosphere and affects  
 232 many aspects of tropical and extratropical weather (Waliser et al., 2009; Zhang et al.,  
 233 2020). Thus, a good emulator of an atmospheric model should replicate the statistical  
 234 characteristics of its MJO.

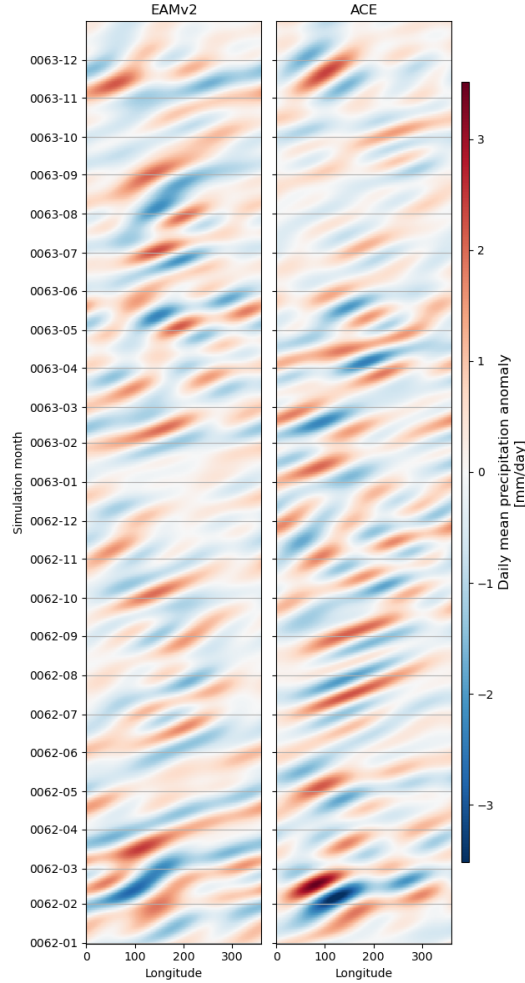


**Figure 5.** Hovmöller diagrams of daily mean tropical-mean precipitation over two typical years, bandpassed to retain 20-100 day periods. Both EAMv2 and ACE show patterns of eastward propagating tropical precipitation anomalies that last around 30 to 90 days.

235 Figure 4 suggests that ACE captures key statistical characteristics of EAMv2’s simulated  
 236 MJO. This skill is more directly verified by isolating the MJO frequency band with a 20-  
 237 100 day bandpass filter to daily- and meridional-mean ( $15^{\circ}\text{S}$ - $15^{\circ}\text{N}$ ) tropical precipita-  
 238 tion anomalies. Figure 5 shows longitude-time Hovmöller diagrams of a typical two year  
 239 segment from ACE and EAMv2 simulations of the 10-year validation period. The band-  
 240 pass filter drives the roughly 50-day period of the features. It is nevertheless impressive  
 241 that ACE (right panel) accurately captures the amplitude and eastward propagation of  
 242 the MJO spatiotemporal evolution simulated by EAMv2 (left panel).

#### 243 4 Conclusions

244 With approximately the same training and testing protocol, ACE emulates EAMv2 with  
 245 excellent skill similar to the FV3GFS model on which ACE was originally trained, as mea-  
 246 sured using 10-year time-mean climatological biases of geographically varying fields such  
 247 as precipitation, near-surface and upper-tropospheric temperature and precipitable wa-  
 248 ter. This suggests that ACE could easily be trained to also emulate other global atmo-  
 249 sphere models.

250 ACE emulates diverse characteristics of EAMv2-simulated precipitation encouragingly  
 251 well. The emulator nearly matches the EAMv2 frequency distribution of daily precip-  
 252 itation out to its extreme-precipitation tail. A Wheeler-Kiladis spectral analysis of trop-  
 253 ical convectively coupled waves also shows good consistency between ACE and EAMv2,  
 254 including in the simulated Madden-Julian Oscillation. That is, ACE captures the space-  
 255 time organization of precipitation simulated by EAMv2.

256 These results were obtained for the important special case of annually-repeating clima-  
 257 tological sea-surface temperatures. It remains to be seen how ACE will fare when faced  
 258 with more realistic time-varying forcing or observational data. Over the longer term, we  
 259 envision integrating future versions of ACE with other conventional or machine-learned  
 260 Earth system components, such as a dynamical ocean, as part of the E3SM ecosystem  
 261 and other climate and earth system models. This would enable coupled climate simu-  
 262 lations or simulation ensembles with greatly reduced computational cost. We also en-  
 263 vision using ACE to emulate finer-grid global atmosphere models, such as DOE’s SCREAM  
 264 (Caldwell et al., 2021), using ML to affordably translate the enhanced fidelity of such  
 265 models into more reliable centennial climate simulations.

## 266 Open Research

### 267 Data Availability Statement

268 ACE model weights (2.5 GB) and the EAMv2 10-year validation set (165 GB) are avail-  
 269 able to download over HTTP from the E3SM project’s NERSC science gateway at [https://](https://portal.nersc.gov/archive/home/projects/e3sm/www/e3smv2-fme-dataset)  
 270 [portal.nersc.gov/archive/home/projects/e3sm/www/e3smv2-fme-dataset](https://portal.nersc.gov/archive/home/projects/e3sm/www/e3smv2-fme-dataset). Doc-  
 271 umentation, inference code, and an example configuration for running ACE are avail-  
 272 able in the following repository: <https://github.com/ai2cm/ace> (Watt-Meyer et al.,  
 273 2023).

### 274 Acknowledgments

275 This research was funded by Laboratory Directed Research and Development (LDRD  
 276 22-ERD-052) at Lawrence Livermore National Laboratory. It was initiated when James  
 277 Duncan was a 2023 summer intern at AI2. The Energy Exascale Earth System Model  
 278 (E3SM) project is funded by the U.S. Department of Energy, Office of Science, Office  
 279 of Biological and Environmental Research. It used computational resources of the E3SM  
 280 project and NERSC, a U.S. Department of Energy Office of Science User Facility located  
 281 at Lawrence Berkeley National Laboratory, using NERSC award BER-ERCAP0024832.  
 282 EAMv2 simulations were performed using a high-performance computing cluster (Chrysalis)  
 283 provided by the BER Earth System Modeling program and operated by the Laboratory  
 284 Computing Resource Center at Argonne National Laboratory. ACE data preprocessing,  
 285 training, and inference runs used NERSC’s Perlmutter system. In addition, we thank  
 286 James Benedict and Walter Hannah of the E3SM project for helpful conversations on  
 287 tropical variability in EAMv2 and for sharing their tropical diagnostics code. Caldwell  
 288 and Golaz’s work was performed under the auspices of the U.S. Department of Energy  
 289 by Lawrence Livermore National Laboratory under Contract DE-AC52-07NA27344.

## 290 References

- 291 Ben-Bouallegue, Z., Weyn, J. A., Clare, M. C. A., Dramsch, J., Dueben, P., &  
 292 Chantry, M. (2023). Improving medium-range ensemble weather forecasts  
 293 with hierarchical ensemble transformers.  
 294 doi: 10.48550/arXiv.2303.17195
- 295 Bi, K., Xie, L., Zhang, H., Chen, X., Gu, X., & Tian, Q. (2023). Accurate medium-  
 296 range global weather forecasting with 3D neural networks. *Nature*, *619*, 533–

- 297 538. doi: 10.1038/s41586-023-06185-3
- 298 Bonev, B., Kurth, T., Hundt, C., Pathak, J., Baust, M., Kashinath, K., & Anandku-  
299 mar, A. (2023). Spherical Fourier neural operators: Learning stable dynamics  
300 on the sphere.  
301 doi: 10.48550/arXiv.2306.03838
- 302 Caldwell, P. M., Terai, C. R., Hillman, B., Keen, N. D., Bogenschutz, P., Lin, W.,  
303 ... Zender, C. S. (2021). Convection-permitting simulations with the E3SM  
304 global atmosphere model. *Journal of Advances in Modeling Earth Systems*, *13*,  
305 e2021MS002544. doi: 10.1029/2021MS002544
- 306 Golaz, J.-C., Van Roekel, L. P., Zheng, X., Roberts, A. F., Wolfe, J. D., Lin, W.,  
307 ... Bader, D. C. (2022). The DOE E3SM Model Version 2: Overview of the  
308 physical model and initial model evaluation. *Journal of Advances in Modeling  
309 Earth Systems*, *14*, e2022MS003156. doi: 10.1029/2022MS003156
- 310 Hannah, W. M., Bradley, A. M., Guba, O., Tang, Q., Golaz, J.-C., & Wolfe, J.  
311 (2021). Separating physics and dynamics grids for improved computational  
312 efficiency in spectral element earth system models. *Journal of Advances in  
313 Modeling Earth Systems*, *13*, e2020MS002419. doi: 10.1029/2020MS002419
- 314 Huffman, G. J., Adler, R. F., Behrangi, A., Bolvin, D. T., Nelkin, E. J., Gu, G., &  
315 Ehsani, M. R. (2023). The new Version 3.2 Global Precipitation Climatol-  
316 ogy Project (GPCP) monthly and daily precipitation products. *Journal of  
317 Climate*, *36*, 7635–7655. doi: 10.1175/JCLI-D-23-0123.1
- 318 IPCC. (2013). *Climate Change 2013: The Physical Science Basis. Contribu-  
319 tion of Working Group I to the Fifth Assessment Report of the Intergov-  
320 ernmental Panel on Climate Change.* Cambridge University Press. doi:  
321 10.1017/CBO9781107415324
- 322 Kingma, D. P., & Ba, J. (2017). Adam: A method for stochastic optimization.  
323 doi: 10.48550/arXiv.1412.6980
- 324 Kucharski, F., Molteni, F., King, M. P., Farneti, R., Kang, I.-S., & Feudale, L.  
325 (2013). On the need of intermediate complexity general circulation models:  
326 A “SPEEDY” example. *Bulletin of the American Meteorological Society*, *94*,  
327 25–30. doi: 10.1175/BAMS-D-11-00238.1
- 328 Lam, R., Sanchez-Gonzalez, A., Willson, M., Wirnsberger, P., Fortunato, M., Alet,  
329 F., ... Battaglia, P. (2023). GraphCast: Learning skillful medium-range global  
330 weather forecasting.  
331 doi: 10.48550/arXiv.2212.12794
- 332 Loeb, N. G., Doelling, D. R., Wang, H., Su, W., Nguyen, C., Corbett, J. G., ...  
333 Kato, S. (2018). Clouds and the Earth’s Radiant Energy System (CERES) En-  
334 ergy Balanced and Filled (EBAF) Top-of-Atmosphere (TOA) Edition-4.0 Data  
335 Product. *Journal of Climate*, *31*, 895–918. doi: 10.1175/JCLI-D-17-0208.1
- 336 Madden, R. A., & Julian, P. R. (1971). Detection of a 40–50 day oscillation in the  
337 zonal wind in the tropical Pacific. *Journal of the Atmospheric Sciences*, *28*,  
338 702–708. doi: 10.1175/1520-0469(1971)028<0702:DOADOI>2.0.CO;2
- 339 Meinshausen, M., Raper, S. C. B., & Wigley, T. M. L. (2011). Emulating coupled  
340 atmosphere-ocean and carbon cycle models with a simpler model, MAGICC6  
341 – Part 1: Model description and calibration. *Atmospheric Chemistry and  
342 Physics*, *11*, 1417–1456. doi: 10.5194/acp-11-1417-2011
- 343 Nguyen, T., Brandstetter, J., Kapoor, A., Gupta, J. K., & Grover, A. (2023). Cli-  
344 maX: A foundation model for weather and climate.  
345 doi: 10.48550/arXiv.2301.10343
- 346 Pathak, J., Subramanian, S., Harrington, P., Raja, S., Chattopadhyay, A., Mar-  
347 dani, M., ... Anandkumar, A. (2022). FourCastNet: A global data-driven  
348 high-resolution weather model using adaptive Fourier neural operators.  
349 doi: 10.48550/arXiv.2202.11214
- 350 Waliser, D., Sperber, K., Hendon, H., Kim, D., Wheeler, M., Weickmann, K., ...  
351 Stern, W. (2009). MJO simulation diagnostics. *Journal of Climate*, *22*,

- 352 3006-3030. doi: 10.1175/2008JCLI2731.1  
353 Watt-Meyer, O., Dresdner, G., McGibbon, J., Duncan, J., Henn, B., Clark, S., &  
354 Perkins, W. A. (2023). Inference code for the AI2 Climate Emulator [Soft-  
355 ware].  
356 doi: 10.5281/zenodo.10463348
- 357 Watt-Meyer, O., Dresdner, G., McGibbon, J., Clark, S. K., Henn, B., Duncan, J.,  
358 ... Bretherton, C. S. (2023). ACE: A fast, skillful learned global atmospheric  
359 model for climate prediction.  
360 doi: 10.48550/arXiv.2310.02074
- 361 Wheeler, M., & Kiladis, G. N. (1999). Convectively coupled equatorial waves:  
362 Analysis of clouds and temperature in the wavenumber–frequency do-  
363 main. *Journal of the Atmospheric Sciences*, *56*, 374–399. doi: 10.1175/  
364 1520-0469(1999)056<0374:CCEWAO>2.0.CO;2
- 365 Zhang, C. (2005). Madden-Julian Oscillation. *Reviews of Geophysics*, *43*. doi: 10  
366 .1029/2004RG000158
- 367 Zhang, C., Adames, A. F., Khouider, B., Wang, B., & Yang, D. (2020). Four  
368 theories of the Madden-Julian Oscillation. *Reviews of Geophysics*, *58*,  
369 e2019RG000685. doi: 10.1029/2019RG000685